Supporting Information

Rigid Donor Units Enable Efficient Multi-Resonance Thermally Activated Delayed Fluorescence Emitters for Narrowband Blue OLEDs

Deli Li, Simin Jiang, Qingchao Liu, Ruizhe Xu, Guo-Xi Yang, Wei Li,* Shi-Jian Su.* Xuchuan Jiang**

Contents

1. Experimental Section

1.1 General Information

Mass spectrum was recorded by an AXIMA-CFRTM plus instrument and a JEOL JMS-K9 mass spectrometer. ^{1}H and ^{13}C NMR spectra were recorded on a Bruker NMR spectrometer operating at 400 and 101 MHz, respectively. UV-vis absorption spectra were recorded using Perkin-Elmer Lambda 950-PKA UV-Vis. Steady-state fluorescent and phosphorescent spectra were recorded by a FluoroMax-4 Spectro-fluorometer (Horiba Jobin Yvon). Photoluminescence quantum yields (PLQYs) in toluene solution and doped films were recorded on an integrating sphere of Hamamatsu absolute PLQY spectrometer (C11347-01). Transient photoluminescence decay spectra and the PLQYs of the thin film samples were evaluated with an Edinburgh FLS980 fluorescence spectrophotometer. Differential scanning calorimetry (DSC) measurements were performed on Netzsch DSC 209 under nitrogen flow at two heating and cooling cycles with a heating rate of 10 °C min^{-1} and a cooling rate of 20 °C min^{-1}. Thermogravimetric analyses (TGA) were performed on Netzsch TG 209 under nitrogen flow at a heating rate of 10 °C min^{-1}. Cyclic voltammetry (CV) was carried out on a CHI600D electrochemical workstation with a platinum working electrode and a platinum wire counter electrode against Ag/AgCl reference electrode with a nitrogen-saturated anhydrous acetonitrile and dichloromethane solution (ratio, 4:1) of 0.1 mol L^{-1} tetrabutylammonium hexafluorophosphate.

1.2 Quantum Chemical Methods

All of the simulations were performed using the Gaussian 16 program package.[1] All the ground state (S_0) geometries were initially optimized using the PBE0 functional with 6-311G(d, p) basis set in vacuum according to density functional theory (DFT). All the excited states were optimized by time-dependent density functional theory (TD-DFT)/B3LYP/6-31G** level in toluene with polarizable continuum model (PCM) based on S_0 geometries. The visualization of HOMO and LUMO of the optimized geometries were using Gview 6.0.16 software, while the hole and particle distribution of natural transition orbitals (NTOs) analysis were conducted by Multiwfn.[2] The ΔE_{ST}s of these molecules were calculated with SCS-CC2 method with MRCC software.[3] The SOC constants between S_n and T_n were calculated by using ORCA program.[4] Reorganization energy and Huang-Rhys (HR) factors were calculated with MOMAP program

based on the optimized geometries.[5]

1.3 Exciton Dynamic Rate Constant Calculation

According to transient decay curves and photoluminescence quantum yield measurement, we can obtain:[6]

$$\emptyset_{PL} = \frac{k_r^S}{k_r^S + k_{nr}^s} \quad (S1)$$

$$\emptyset_{PF} = \frac{k_r^S}{k_r^S + k_{nr}^S + k_{isc}} = k_r^S \tau_{PF} \quad (S2)$$

$$\emptyset_{ISC} = 1 - \emptyset_{PF} \quad (S3)$$

$$k_{isc} = \frac{\emptyset_{TADF}}{\emptyset_{TADF} + \emptyset_{PF}} k_r^S \quad (S4)$$

$$k_{PF} = \frac{1}{\tau_{PF}} \quad (S5)$$

$$k_{DF} = \frac{1}{\tau_{TADF}} \quad (S6)$$

$$k_{TADF} = \frac{\emptyset_{TADF}}{\emptyset_{ISC} \tau_{TADF}} \quad (S7)$$

In which, $\emptyset_{PL}, \emptyset_{PF}, \emptyset_{TADF}, \emptyset_{ISC}$ represent photoluminescence quantum yield (PLQY), quantum yield of prompt component, quantum yield of delayed component, intersystem crossing ratio, respectively. $k_r^S, k_{nr}^S, k_{isc}, k_{PF}, k_{DF}, k_{risc}, k_{TADF}$ represent radiative, non-radiative, prompt process, delay process, intersystem crossing rate constants, reverse intersystem crossing, and thermally activated delayed fluorescence (TADF) rate constants, respectively.

1.4 Device Fabrication and Characterization

All the organic materials for device fabrication were available from ***Luminescence Technology Corp.*** and ***Xi'an Yuri Solar Co., Ltd***. Glass substrates pre-coated with a 95-nm-thin layer of indium tin oxide (ITO) with a sheet resistance of 10 Ω per square were thoroughly cleaned in ultrasonic bath of tetrahydrofuran, isopropyl alcohol, detergent, deionized water, and isopropyl alcohol and treated with O_2 plasma for 10 min in sequence. Organic layers were deposited onto the ITO-coated glass substrates by thermal evaporation under high vacuum (~10^{-5} Pa). Cathode was patterned using a shadow mask with an array of 3 mm × 3 mm openings. Deposition rates are 1 − 2 Å s^{-1} for organic materials, 0.1 Å s^{-1} for LiF, and 6 Å s^{-1} for aluminum,

respectively. Electroluminescence (EL) spectra were recorded by Photo Research PR745. The current density and luminance versus driving voltage characteristics were measured by Keithley 2450 and PR745. External quantum efficiencies (EQEs) were calculated from the current density, luminance, and EL spectra, assuming a Lambertian distribution.

2. Thermal Properties and Energy Levels

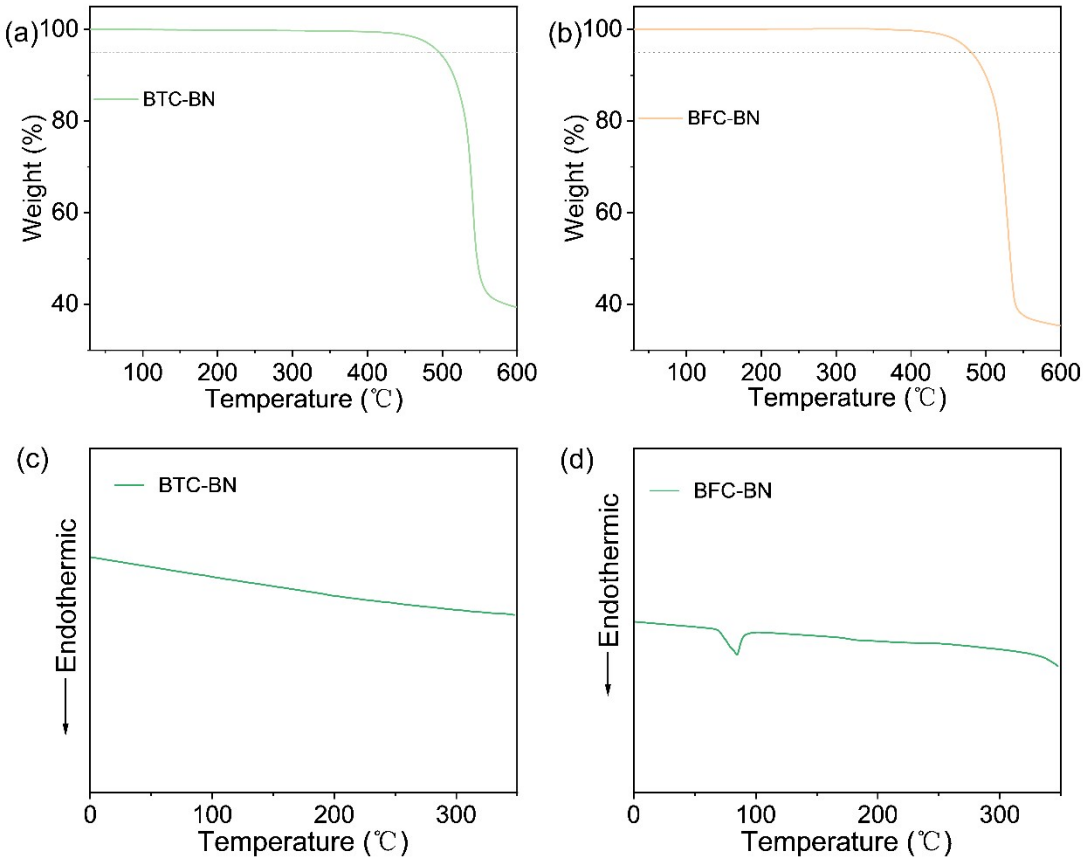

Figure S1. TGA and DSC curves of BTC-BN (a, c) and BFC-BN (b, d).

3. Theoretical Calculation

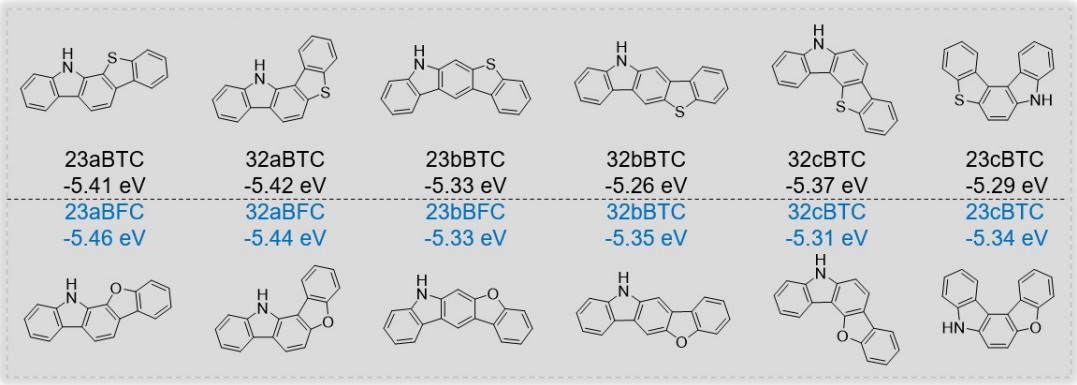

Figure S2. Calculated HOMO energy levels of benzothienocarbazole and benzofurocarbazole groups.

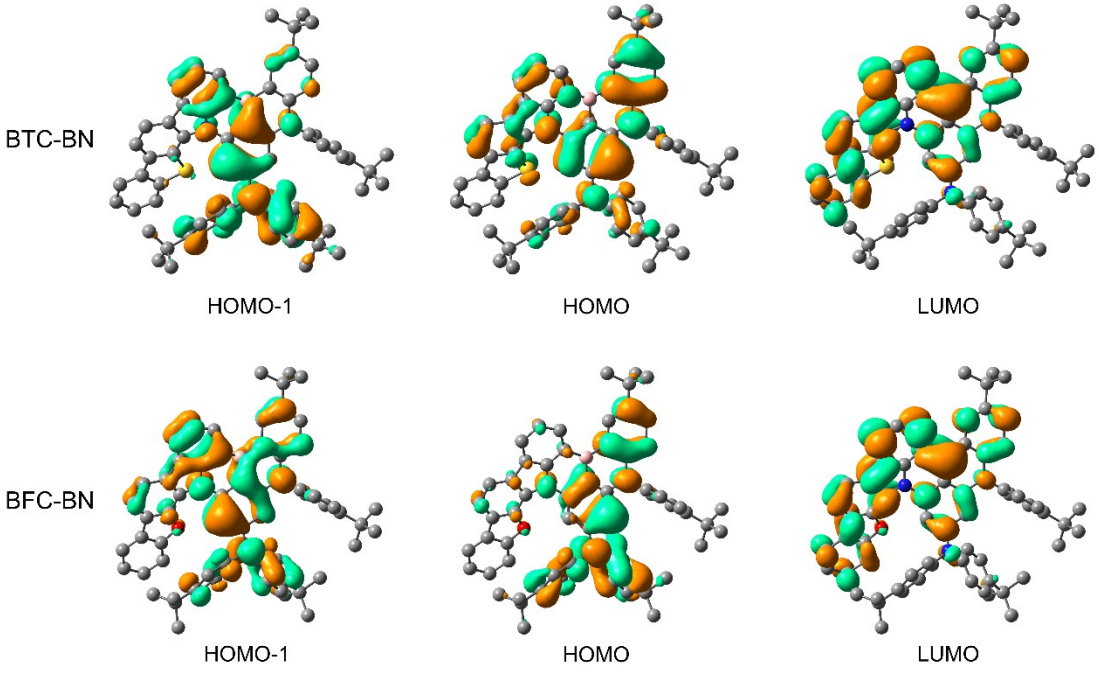

Figure S3. HOMO-1, HOMO and LUMO distributions of BTC-BN and BFC-BN.

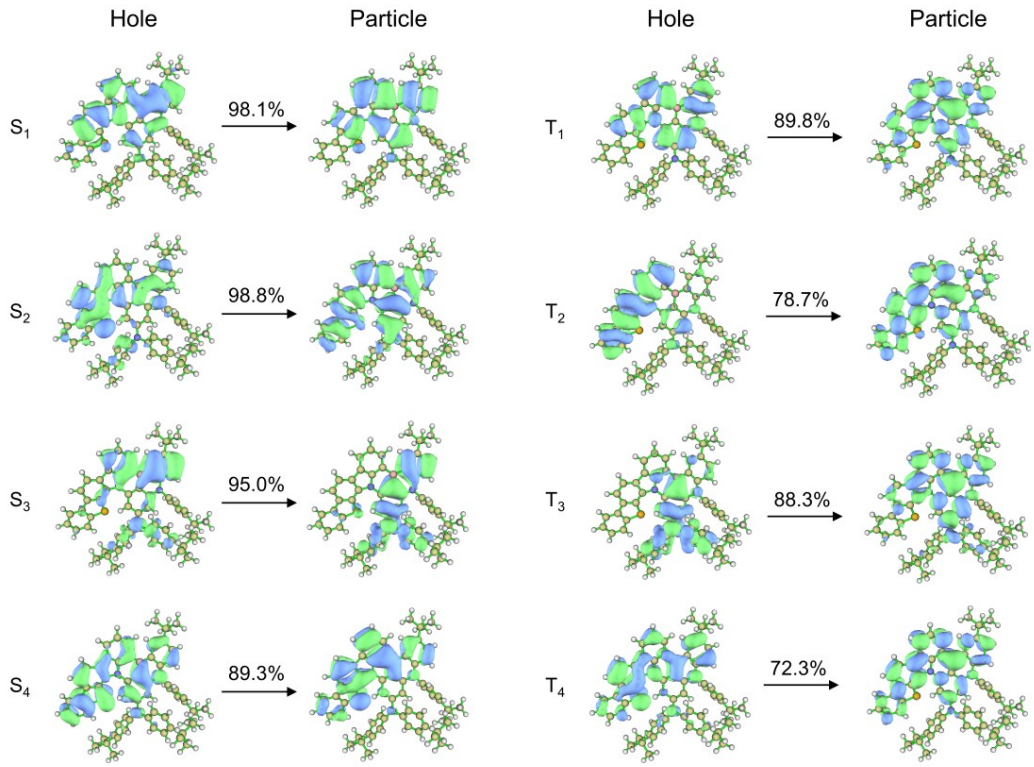

Figure S4. Natural transition orbitals (NTOs) for the excited singlet (S_n) and triplet (T_m) states for BTC-BN. NTOs for S_n and T_m were calculated at the B3LYP/6-31g* level.

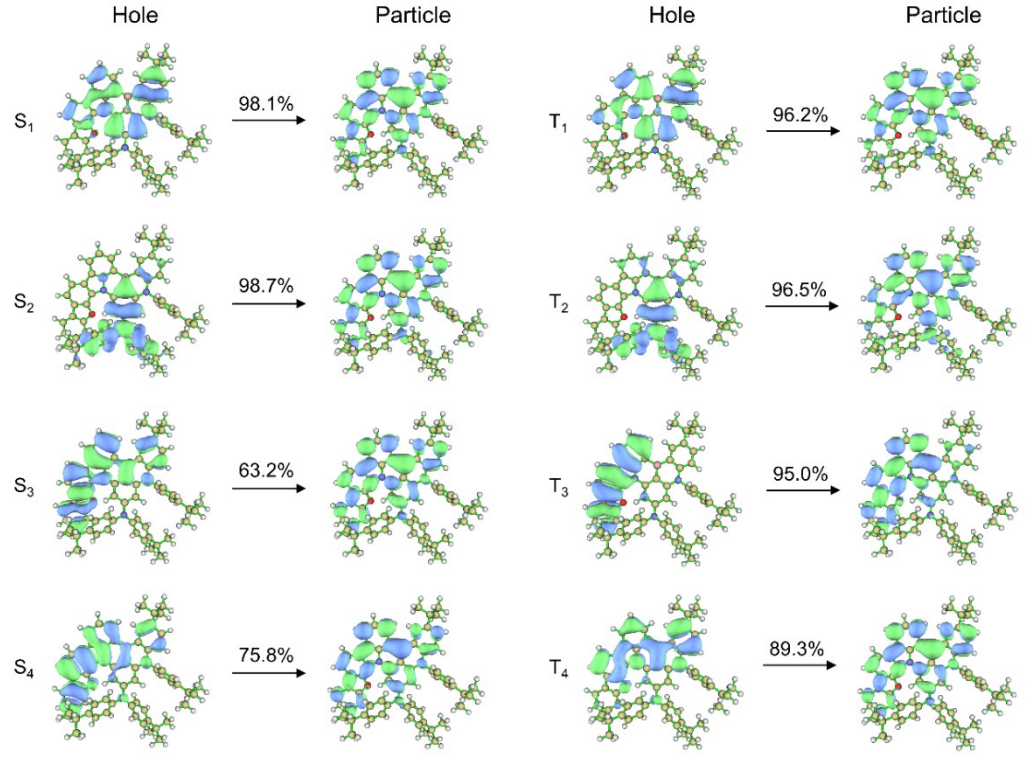

Figure S5. Natural transition orbitals (NTOs) for the excited singlet (S_n) and triplet (T_m) states for BFC-BN. NTOs for S_n and T_m were calculated at the B3LYP/6-31g* level.

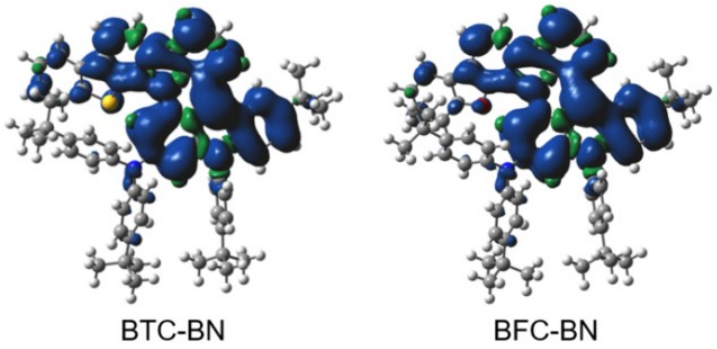

Figure S6. Triplet spin density distribution (TSDD) of BTC-BN and BFC-BN.

Table S1. SOCME of BTC-BN and BFC-BN between S_1, S_2 and T_m (m=1, 2, 3, 4) states.

Emitters	$\langle S_1 \lvert \hat{H}_{SOC} \rvert T_1 \rangle$	$\langle S_1 \lvert \hat{H}_{SOC} \rvert T_2 \rangle$	$\langle S_1 \lvert \hat{H}_{SOC} \rvert T_3 \rangle$	$\langle S_1 \lvert \hat{H}_{SOC} \rvert T_4 \rangle$
BTC-BN	0.34	0.14	0.87	1.30
BFC-BN	0.07	0.04	0.20	0.17
	$\langle S_2 \lvert \hat{H}_{SOC} \rvert T_1 \rangle$	$\langle S_2 \lvert \hat{H}_{SOC} \rvert T_2 \rangle$	$\langle S_2 \lvert \hat{H}_{SOC} \rvert T_3 \rangle$	$\langle S_2 \lvert \hat{H}_{SOC} \rvert T_4 \rangle$
BTC-BN	0.35	0.53	0.28	0.12
BFC-BN	0.08	0.13	0.05	0.23

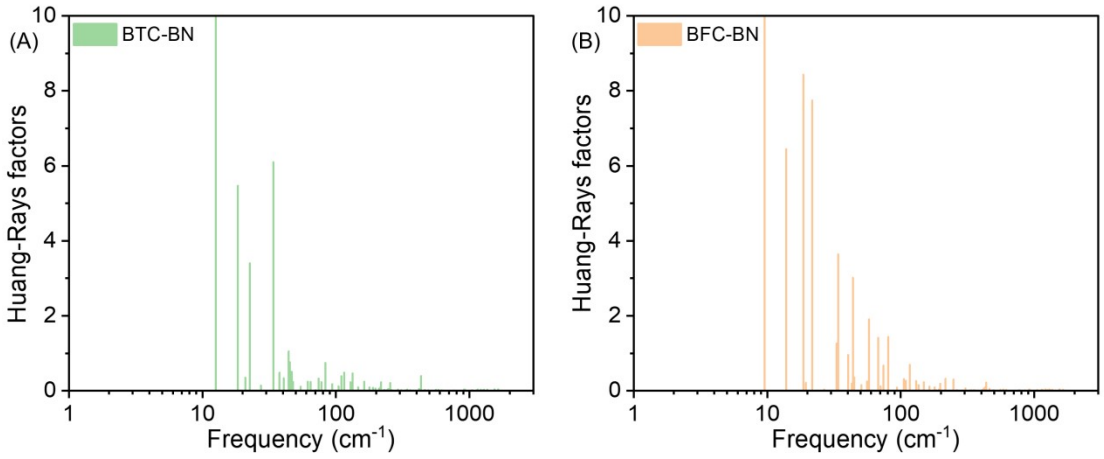

Figure S7. Calculated Huang-Rhys (HR) factor for the $S_1 \rightarrow S_0$ transition of BTC-BN and BFC-BN.

Table S2. Configuration interaction description of FMO transition of BTC-BN and BFC-BN based on optimized ground state geometry calculated on PBE0/6-31G** level in toluene solution employing PCM model.

Molecules	States	Energy (eV)	*f*	CI description
BTC-BN	S_1	2.9761	0.3128	H -> L 82.9%, H-1 -> L 14.4%
	S_2	3.1010	0.2611	H-1 -> L 81.3%, H -> L 14.5%
	T_1	2.5399		H -> L 45.6%, H-1 -> L 29.3%, H-3 -> L 10.2%
	T_2	2.6981		H-3 -> L 34.0%, H -> L 30.3%, H-3 -> L+1 7.0%, H-1 -> L 6.9%
	T_3	2.7708		H-1 -> L 49.2%, H-3 -> L 20.0%, H-3 -> L+1 6.0%
BFC-BN	S_1	2.9843	0.3902	H-1 -> L 88.0%, H -> L 9.0%
	S_2	3.0450	0.2444	H -> L 88.5%, H-1 -> L 8.7%
	T_1	2.5354		H-1 -> L 74.3%, H -> L 7.2%, H-2 -> L 7.1%
	T_2	2.7086		H -> L 62.8%, H-2 -> L 12.5%
	T_3	2.7715		H-2 -> L 43.5%, H-1 -> L 16.2%, H-2 -> L+1 11.4%, H -> L 7.2%

Table S3. Configuration interaction description of FMO transition of BTC-BN based on optimized ground state geometry calculated on the functionals with different HF exchange percentage (HF%) in toluene solution employing PCM model.

Functionals	Excited states	Energy (eV)	*f*	CI description
B3LYP (20%HF)	S_1	2.8626	0.2637	H -> L 92.1%, H-1 -> L 6.2%
	S_2	2.9779	0.2524	H-1 -> L 90.4%, H -> L 6.4%
PBE0 (25%HF)	S_1	2.9761	0.3128	H -> L 82.9%, H-1 -> L 14.4%
	S_2	3.1010	0.2611	H-1 -> L 81.3%, H -> L 14.5%
MPW1B95 (31%HF)	S_1	3.0569	0.3731	H -> L 72.8%, H-1 -> L 22.9%
	S_2	3.2135	0.2692	H-1 -> L 70.7%, H -> L 22.7%
BMK (42%HF)	S_1	3.2390	0.4552	H -> L 63.5%, H-1 -> L 29.8%
	S_2	3.4539	0.3173	H-1 -> L 59.8%, H -> L 28.0%
M06-2X (56%HF)	S_1	3.3771	0.5067	H -> L 59.4%, H-1 -> L 30.1%
	S_2	3.6423	0.3428	H-1 -> L 51.9%, H -> L 26.5%

Table S4. Configuration interaction description of FMO transition of BFC-BN based on optimized ground state geometry calculated on the functionals with different HF exchange percentage (HF%) in toluene solution employing PCM model.

Functionals	Excited states	Energy (eV)	*f*	CI description
B3LYP	S_1	2.8825	0.3544	H-1 -> L 80.9%, H -> L 16.9%
(20%HF)	S_2	2.9089	0.2172	H -> L 81.6%, H-1 -> L 16.5%
PBE0	S_1	2.9761	0.3128	H -> L 82.9%, H-1 -> L 14.4%
(25%HF)	S_2	3.1010	0.2444	H-1 -> L 81.3%, H -> L 14.5%
MPW1B95	S_1	3.0497	0.4219	H-1 -> L 84.7%, H -> L 11.3%
(31%HF)	S_2	3.1713	0.2822	H -> L 84.2%, H-1 -> L 10.8%
BMK	S_1	3.2214	0.4895	H-1 -> L 76.8%, H -> L 17.3%
(42%HF)	S_2	3.4266	0.3562	H -> L 73.6%, H-1 -> L 16.1%
M06-2X	S_1	3.3527	0.5266	H-1 -> L 54.0%, H -> L 36.7%
(56%HF)	S_2	3.6378	0.4161	H -> L 48.7%, H-1 -> L 31.7%

4. Photophysical Properties

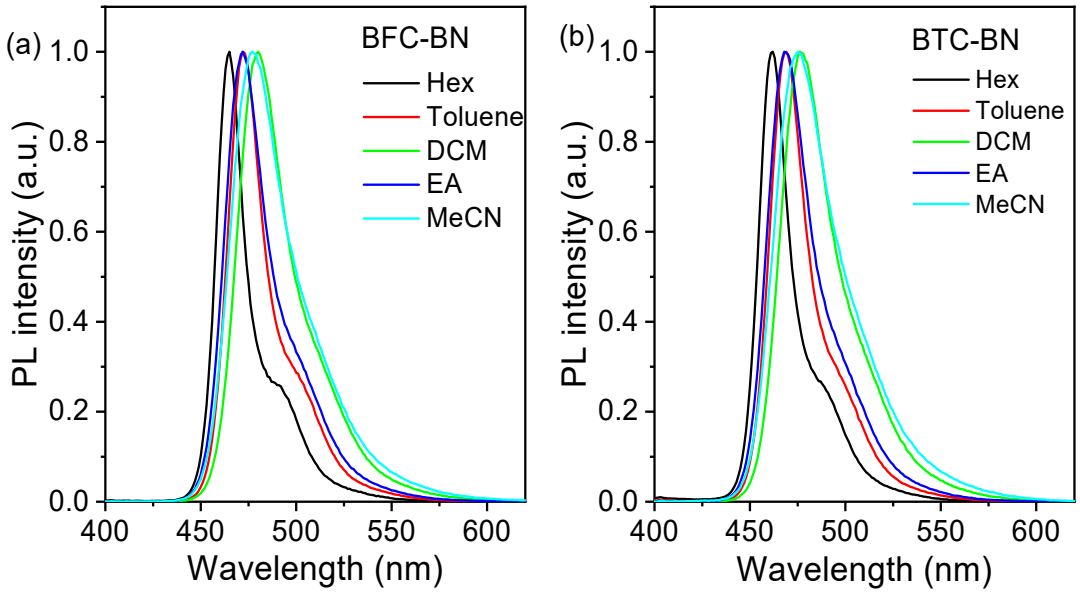

Figure S8. PL spectra of BFC-BN (a) and BTC-BN (b) in different solvents measured at 300 K.

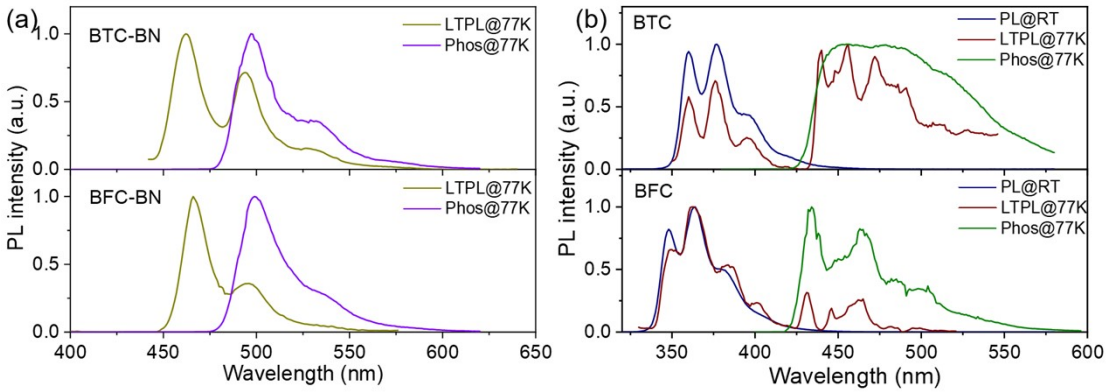

Figure S9. Low-temperature PL spectra and phosphorescence spectra of BFC-BN, BTC-BN (a), and BTC and BFC donor (b) units measured in frozen toluene at 77 K.

The PL spectra of BTC and BFC donor were measured in dilute toluene, with the emission peak of 360 and 377 nm for BTC, and 348 and 364 nm for BFC. The fluorescence and phosphorescence spectra of BTC and BFC donor units were recorded under 77 K in oxygen-free frozen toluene. The singlet and triplet energy levels are estimated to be 3.44 and 2.82 eV for BTC, and 3.65 and 2.86 eV for BFC, from the emission peak. Consequently, the ΔE_{ST}s of BTC and BFC donor were calculated to be 0.62 and 0.79 eV, respectively.

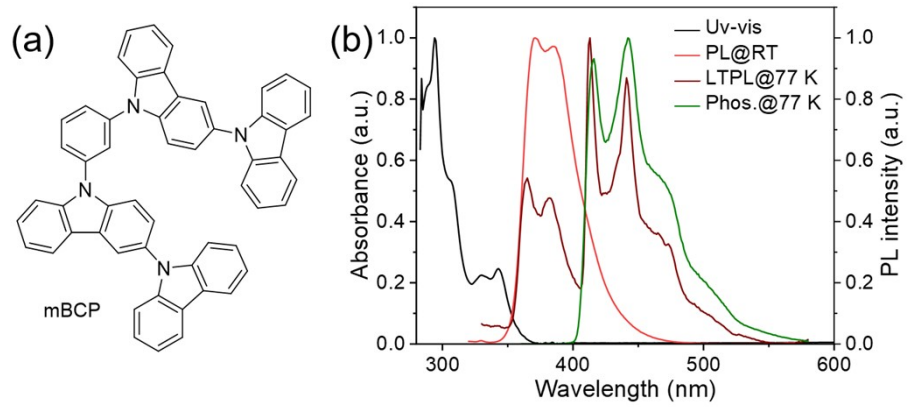

Figure S10. (a) Chemical structure of mBCP. (b) UV-vis and PL spectra in toluene measured at 300 K and low-temperature PL spectra and phosphorescence spectra measured in frozen toluene at 77 K.

Ultraviolet–visible (UV-vis) absorption and photoluminescence (PL) spectra of mBCP were preliminarily characterized in dilute toluene solution (1×10^{-5} M). Figure S7 show that the absorption band peaking at 330 and 343 nm corresponding to the n–π* transition of the carbazole moiety. The optical bandgap (E_g) is estimated to be 3.46 eV from the onset of the absorption spectra. The HOMO energy level of mBCP was estimated to be -5.87 eV measured by ultraviolet photoelectron spectroscopy (Fig. S12), and the LUMO energy level was calculated to be -2.41 eV. The PL spectra present a purple–blue emission of mBCP with the emission peak wavelength at 370 and a shoulder peak at 385 nm. The fluorescence and phosphorescence spectra are recorded under 77 K in oxygen-free frozen toluene. The estimated singlet and triplet energy levels are 3.40 and 3.00 eV, respectively, both higher than those of BTC-BN and BFC-BN, and suitable to serve as the host materials of these emitters.

Table S5. Photo-physics properties of mBCP.

Molecule	λ_{abs} [nm]	λ_{em} [nm]	E_g [eV]	HOMO/LUMO [eV][a]	S_1 [b] [eV]	T_1 [b] [eV]
mBCP	343	370/385	3.46	-5.87/-2.41	3.40	3.00

[a)] HOMO energy level was determined from ultraviolet photo-electron spectroscopy, LUMO= HOMO + E_g. [b)] Singlet and triplet energy estimated from the peak of the fluorescence and phosphorescence spectrum in a frozen toluene matrix (1×10^{-5} M, 77 K).

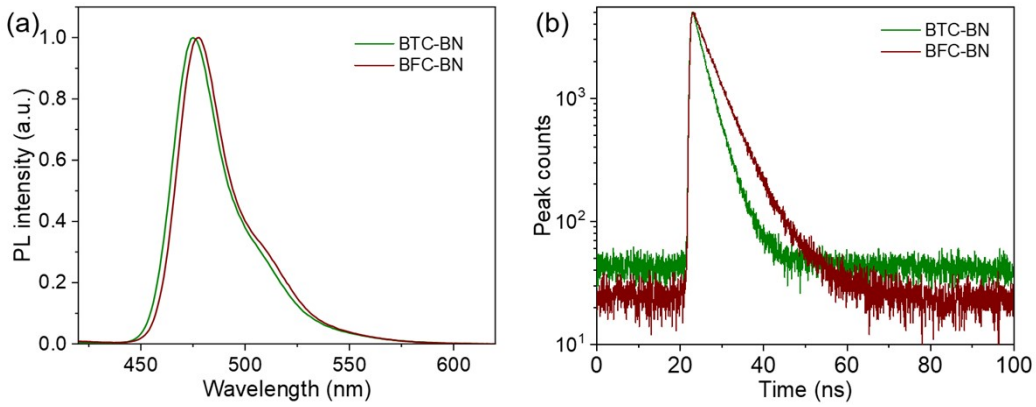

Figure S11. PL spectra (a) and transient PL decay curves (b) of BTC-BN and BFC-BN in mBCP host with the doping concentration of 3 wt%.

Table S6. Photo-physics properties of BFC and BTC in mBCP host.

Emitter	PLQY [%]	τ_{PF} [ns]	τ_{DF} [μs]	ϕ_{PF} [%]	ϕ_{DF} [%]	k_r^s [$\sim 10^7$ s^{-1}]	k_{ISC} [$\sim 10^8$ s^{-1}]	k_{RISC} [$\sim 10^4$ s^{-1}]	k_{nr}^T [$\sim 10^2$ s^{-1}]	k_{CQ} [$\sim 10^2$ s^{-1}]
BFC-BN	94.6	4.7	88.7	21.2	73.4	4.5	1.7	5.0	7.7	7.8
BTC-BN	96.8	3.8	50.3	34.1	62.7	9.0	1.7	5.5	9.7	9.7

5. Energy Levels

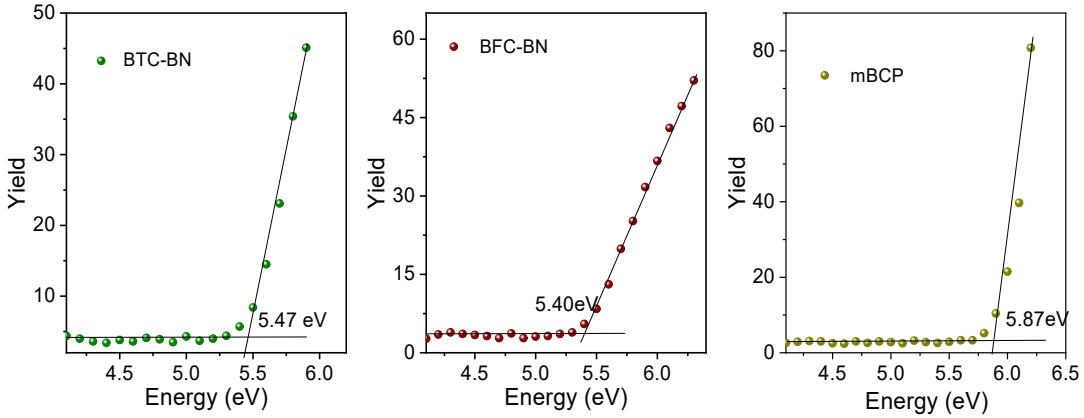

Figure S12. Atmospheric ultraviolet photoelectron spectroscopies of BTC-BN, BFC-BN and mBCP films.

6. OLED Performances

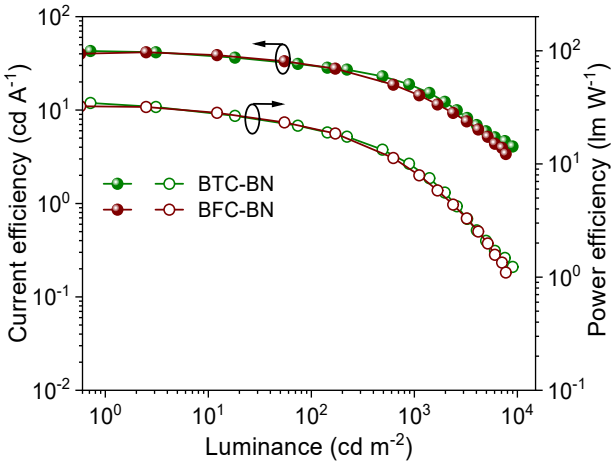

Figure S13 Current efficiency and Power efficiency curves of BTC-BN and BFC-BN based devices.

7. Synthesis

All the reagents were purchased from *Energy Chemical Co., Bidepharm Ltd. Co*., and used as received without further purification.

7.1 Synthesis of BTC-BN and BFC-BN.

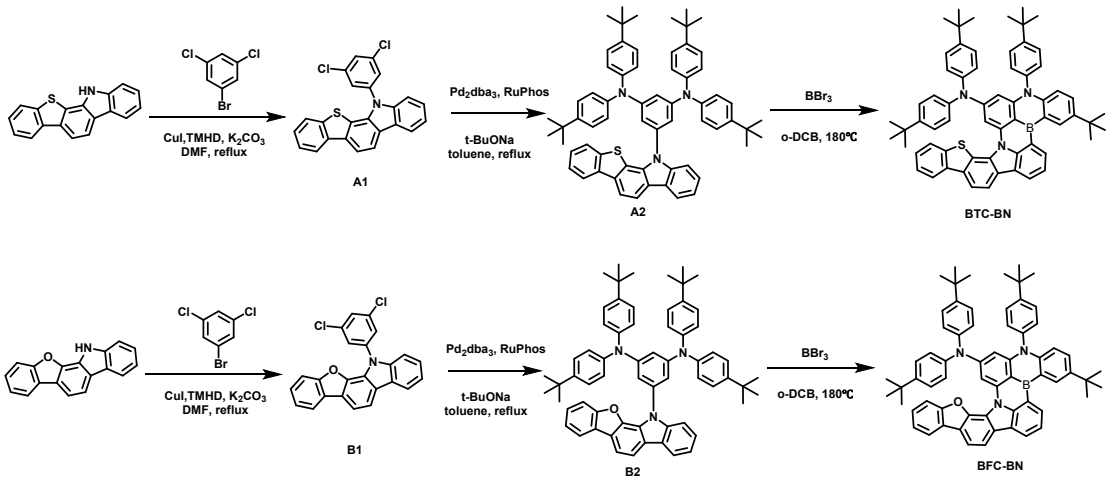

Synthesis of 12-(3,5-dichlorophenyl)-12*H*-benzo[4,5]thieno[2,3-a]carbazole (A1) and 12-(3,5-dichlorophenyl)-12*H*-benzofuro[2,3-a]carbazole (B1): 12*H*-benzo[4,5]thieno[2,3-a]carbazole (BTC) or 12*H*-benzofuro[2,3-a]carbazole (BFC) (8.9 mmol), CuI (168.6 mg, 0.86 mmol), 2,2,6,6-tetramethylheptane-3,5-dione (TMHD) (326.3 mg, 1.8 mmol), and K_2CO_3 (2.45 g, 17.7 mmol) were added into a 100 mL three-necked flask followed by addition of DMF (50 mL). The reaction was carried out for 24 h at 165 ℃. After cooling, the mixture was diluted with dichloromethane (DCM) and filtered with celite/silica gel filter. The filtrate was concentrated through a rotary evaporator and adsorbed on silica gel. The product was purified using column chromatography with an eluent of PE: DCM. The separated product was dissolved into chloroform and methanol was added for precipitation. After drying in the vacuum oven, a white powder was obtained. 12-(3,5-dichlorophenyl)-12*H*-benzo[4,5]thieno[2,3-a]carbazole (A1): 3.2 g, Yield 87.8%. HRMS: calcd for $C_{24}H_{13}Cl_2NS$, 417.0146, found 417.0136 $[M]^+$. 12-(3,5-dichlorophenyl)-12*H*-benzofuro[2,3-a]carbazole (B1): 3.1 g, Yield 87%. HRMS: calcd for $C_{24}H_{13}Cl_2NO$, 401.0374, found 401.0368 $[M]^+$.

Synthesis of 5-(12*H*-benzo[4,5]thieno[2,3-*a*]carbazol-12-yl)-*N*^{1},*N*^{1},*N*^{3},*N*^{3}-tetrakis(4-(tert-butyl)phenyl)benzene-1,3-diamine (A2) and 5-(12*H*-benzofuro[2,3-*a*]carbazol-12-yl)-*N*^{1},*N*^{1},*N*^{3},*N*^{3}-tetrakis(4-(*tert*-butyl)phenyl)benzene-1,3-diamine (B2): Bis(4-(tert-

butyl)phenyl)amine (2.9 g, 10.4 mmol), A1 or B1 (5 mmol), tris(dibenzylideneacetone)dipalladium ($Pd_2(dba)_3$, 0.5 g, 0.5 mmol), 2-Dicyclohexylphosphino-2',6'-diisopropoxy-1,1'-biphenyl (RuPhos) (0.46 g, 1 mmol) and sodium *tert*-butoxide (NaOtBu, 1.90 g, 19.9 mmol) were added into a 250 mL three neck round-bottomed flask followed by slow addition of toluene (80 mL). The reaction mixture was stirred and refluxed during 18 h under a nitrogen atmosphere. After completion of the reaction, the reaction mixture was slowly cooled to room temperature and diluted with 160 mL of DCM, then, the mixture was filtered with celite/silica gel filter and concentrated through a rotary evaporator. The mixture was purified through column chromatography with an eluent of PE/DCM. The product was obtained as a white solid. 5-(12*H*-benzo[4,5]thieno[2,3-*a*]carbazol-12-yl)-N^1,N^1,N^3,N^3-tetrakis(4-(*tert*-butyl)phenyl)benzene-1,3-diamine (A2): 3.9 g, Yield 89.8%. HRMS: calcd for $C_{64}H_{65}N_3S$, 907.4899, found 907.4890 $[M]^+$. 5-(12*H*-benzofuro[2,3-*a*]carbazol-12-yl)-N^1,N^1,N^3,N^3-tetrakis(4-(*tert*-butyl)phenyl)benzene-1,3-diamine (B2): 4.0 g, Yield 90.2%. HRMS: calcd for $C_{64}H_{65}N_3O$, 891.5128, found 891.5136 $[M]^+$.

Synthesis of BTC-BN and BFC-BN: Boron tribromide (4.04 g, 16 mmol) and A2 or B2 (4.0 mmol) were dissolved *o*-dichlorobenzene (10 mL) under a nitrogen atmosphere. After stirring at 120 °C for 16 h, the reaction mixture was allowed to cool to room temperature and residual hydrogen iodide was removed in vacuo. After phosphorus buffer solution (pH 7, 20 mL) was added to the reaction mixture, the aqueous layer was separated and extracted with dichloromethane (100 mL, four times). The combined organic layers were washed with brine (60 mL), and dried over magnesium sulfate. After the solvent was removed in vacuo, the crude product was purified through column chromatography with an eluent of PE/DCM to obtain the title compound as a yellow solid.

BTC-BN: ^{1}H NMR (400 MHz, $CDCl_3$) δ 8.86 (d, J = 2.5 Hz, 1H), 8.77 – 8.70 (m, 1H), 8.30 (dd, J = 7.6, 1.1 Hz, 1H), 8.22 (d, J = 8.1 Hz, 1H), 8.18 – 8.10 (m, 2H), 7.79 – 7.70 (m, 1H), 7.66 (t, J = 7.4 Hz, 1H), 7.51 (dd, J = 7.9, 2.1 Hz, 3H), 7.46 (s, 1H), 7.44 – 7.39 (m, 2H), 7.16 – 7.05 (m, 8H), 6.71 (d, J = 9.0 Hz, 1H), 6.19 (s, 1H), 1.47 (s, 9H), 1.36 (s, 9H), 1.12 (s, 18H). ^{13}C NMR (101 MHz, $CDCl_3$) δ 151.40, 151.28, 148.39, 146.66, 145.81, 144.86, 144.06, 142.85, 142.15, 139.12, 137.99, 135.55, 135.39, 134.69, 132.11, 131.05, 129.47, 128.98, 127.36, 126.28, 126.17, 125.65, 125.63, 124.85, 124.27, 123.83, 123.19, 122.35, 122.16, 121.93, 121.28, 117.03, 116.90, 116.25,

101.84, 101.56, 34.74, 34.32, 34.16, 31.66, 31.47, 31.21. HRMS: calcd for $C_{64}H_{62}BN_3S$, 915.4758, found 915.4820 $[M]^+$.

BFC-BN: ^{1}H NMR (400 MHz, $CDCl_3$) δ 8.95 (d, *J* = 2.4 Hz, 1H), 8.88 – 8.79 (m, 1H), 8.54 (d, *J* = 1.7 Hz, 1H), 8.33 (dd, *J* = 7.6, 1.0 Hz, 1H), 8.14 (d, *J* = 8.0 Hz, 1H), 7.91 (td, *J* = 5.4, 4.6, 2.1 Hz, 2H), 7.67 (t, *J* = 7.5 Hz, 1H), 7.55 – 7.46 (m, 3H), 7.30 (ddd, *J* = 5.8, 3.1, 1.9 Hz, 2H), 7.14 (dq, *J* = 16.7, 8.6 Hz, 11H), 7.06 – 7.02 (m, 1H), 6.70 (d, *J* = 9.0 Hz, 1H), 6.20 (d, *J* = 1.7 Hz, 1H), 1.48 (s, 9H), 1.36 (s, 9H), 1.16 (s, 18H). ^{13}C NMR (101 MHz, $CDCl_3$) δ 154.69, 151.87, 151.41, 148.49, 145.91, 145.79, 144.76, 143.97, 143.39, 142.36, 142.10, 139.26, 132.44, 131.00, 129.50, 129.12, 127.43, 127.33, 126.24, 125.86, 124.60, 124.50, 124.01, 123.88, 123.52, 122.89, 122.28, 121.95, 119.82, 116.92, 115.91, 115.50, 114.72, 112.44, 103.47, 103.15, 34.78, 34.39, 34.19, 31.72, 31.51, 31.34. HRMS: calcd for $C_{64}H_{62}N_3OB$, 899.4986, found 899.4990 $[M]^+$.

7.2 Synthesis of 1,3-di(9*H*-[3,9'-bicarbazol]-9-yl)benzene (mBCP).

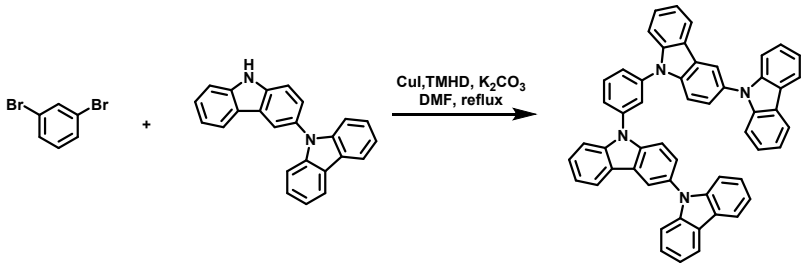

1,3-dibromobenzene (1.00 g, 4.24 mmol), 9*H*-3,9'-bicarbazole (2.96 g, 8.90 mmol), CuI (80.7 mg, 0.43 mmol), 2,2,6,6-tetramethylheptane-3,5-dione (TMHD) (156.2 mg, 0.85 mmol), and K_2CO_3 (2.34 g, 17.0 mmol) were added into a 100 mL three-necked flask followed by addition of DMF (50 mL). The reaction was carried out for 24 h at 165 ℃. After cooling, the mixture was diluted with DCM and filtered with celite/silica gel filter. The filtrate was concentrated through a rotary evaporator and adsorbed on silica gel. The product was purified using column chromatography with an eluent of PE: DCM. The separated product was dissolved into chloroform and methanol was added for precipitation. After drying in the vacuum oven, a white powder was obtained (2.80 g, Yield 89.4%). Further purification was done by train sublimation for vacuum deposition. ^{1}H NMR (400 MHz, $CDCl_3$) δ 8.30 (d, *J* = 2.0 Hz, 2H), 8.17 (d, *J* = 7.8 Hz, 4H), 8.12 (d, *J* = 7.8 Hz, 2H), 8.01 – 7.91 (m, 2H), 7.83 (dd, *J* = 8.1, 2.0 Hz, 2H), 7.74 (d, *J* = 8.6 Hz, 2H), 7.65 – 7.56 (m, 4H), 7.55 – 7.47 (m, 2H), 7.39 (d, *J* = 4.0 Hz, 8H), 7.37 – 7.25 (m, 6H). ^{13}C NMR

(101 MHz, $CDCl_3$) δ 141.79, 141.29, 139.69, 139.27, 131.62, 130.38, 126.94, 126.25, 125.88, 125.76, 125.40, 124.70, 123.20, 123.14, 120.87, 120.79, 120.30, 119.67, 110.77, 110.00, 109.74. HRMS: calcd for $C_{54}H_{34}N_4$, 738.2783, found 738.2779 $[M]^+$.

8. References

[1] M. J. Frisch, G. W. Trucks, H. B. Schlegel, G. E. Scuseria, M. A. Robb, J. R. Cheeseman, G. Scalmani, V. Barone, G. A. Petersson, H. Nakatsuji, X. Li, M. Caricato, A. V. Marenich, J. Bloino, B. G. Janesko, R. Gomperts, B. Mennucci, H. P. Hratchian, J. V. Ortiz, A. F. Izmaylov, J. L. Sonnenberg, Williams, F. Ding, F. Lipparini, F. Egidi, J. Goings, B. Peng, A. Petrone, T. Henderson, D. Ranasinghe, V. G. Zakrzewski, J. Gao, N. Rega, G. Zheng, W. Liang, M. Hada, M. Ehara, K. Toyota, R. Fukuda, J. Hasegawa, M. Ishida, T. Nakajima, Y. Honda, O. Kitao, H. Nakai, T. Vreven, K. Throssell, J. A. Montgomery Jr., J. E. Peralta, F. Ogliaro, M. J. Bearpark, J. J. Heyd, E. N. Brothers, K. N. Kudin, V. N. Staroverov, T. A. Keith, R. Kobayashi, J. Normand, K. Raghavachari, A. P. Rendell, J. C. Burant, S. S. Iyengar, J. Tomasi, M. Cossi, J. M. Millam, M. Klene, C. Adamo, R. Cammi, J. W. Ochterski, R. L. Martin, K. Morokuma, O. Farkas, J. B. Foresman, D. J. Fox, Wallingford, CT 2016.

[2] T. Lu, F. Chen, *J. Comput. Chem.* **2012**, 33, 580.

[3] M. Kallay, P. R. Nagy, D. Mester, Z. Rolik, G. Samu, J. Csontos, J. Csoka, P. B. Szabo, L. Gyevi-Nagy, B. Hegely, I. Ladjanszki, L. Szegedy, B. Ladoczki, K. Petrov, M. Farkas, P. D. Mezei, A. Ganyecz, *J. Chem. Phys.* **2020**, 152, 074107.

[4] F. Neese, *WIREs Comput. Mol. Sci.* **2011**, 2, 73.

[5] a) Z. Shuai, *Chin. J. Chem.* **2020**, 38, 1223; b) Z. Shuai, Q. Peng, *Natl. Sci. Rev.* **2017**, 4, 224.

[6] a) Y. Tao, K. Yuan, T. Chen, P. Xu, H. Li, R. Chen, C. Zheng, L. Zhang, W. Huang, *Adv. Mater.* **2014**, 26, 7931; b) D. Li, M. Li, W. Li, W. Li, Z. Chen, X. Peng, D. Liu, G.-X. Yang, S. Jiang, Y. Gan, Z. Yang, K. Liu, S.-J. Su, *Chem. Eng. J.* **2023**, 458, 141416.